Optics Letters

Orbital angular momentum beams generated by passive dielectric phase masks and their performance in a communication link

Zhe Wang,[1,*] Yan Yan,[1] Amir Arbabi,[2] Guodong Xie,[1] Cong Liu,[1] Zhe Zhao,[1] Yongxiong Ren,[1] Long Li,[1] Nisar Ahmed,[1] Asher J. Willner,[1] Ehsan Arbabi,[2] Andrei Faraon,[2] Robert Bock,[3] Solyman Ashrafi,[4] Moshe Tur,[5] and Alan E. Willner[1]

[1]Department of Electrical Engineering, University of Southern California, Los Angeles, California 90089, USA
[2]T. J. Watson Laboratory of Applied Physics, California Institute of Technology, 1200 E California Blvd., Pasadena, California 91125, USA
[3]R-DEX Systems, Inc., Marietta, Georgia 30068, USA
[4]NxGen Partners, Dallas, Texas 75219, USA
[5]School of Electrical Engineering, Tel Aviv University, Ramat Aviv 69978, Israel
*Corresponding author: wang719@usc.edu

Received 29 May 2017; revised 15 June 2017; accepted 16 June 2017; posted 19 June 2017 (Doc. ID 296912); published 10 July 2017

We demonstrate the generation of orbital angular momentum (OAM) beams using high-efficient polarization-insensitive phase masks. The OAM beams generated by the phase masks are characterized in terms of their tolerance to misalignment (lateral displacement or tilt) between the incident beam and phase mask. For certain scenarios, our results show that (a) when the tilt angle is within the range of −20 to +20 deg, the crosstalk among modes is less than −15 dB; and (b) lateral displacement of 0.3 mm could cause a large amount of power leaked to adjacent modes. Finally, OAM beams generated by the phase masks are demonstrated over a two-channel OAM-multiplexing link, each channel carrying a 40 Gbit/s data stream. An optical signal-to-noise-ratio (OSNR) penalty of ∼1 dB is measured without crosstalk at the bit error rate (BER) of 3.8×10^{-3}. With crosstalk, an OSNR penalty of <1.5 dB is observed at the same BER.

OCIS codes: (060.2605) Free-space optical communication; (080.4865) Optical vortices; (060.4230) Multiplexing.

https://doi.org/10.1364/OL.42.002746

Orbital angular momentum (OAM) modes have gained interest due to their potential to enhance the capacity and spectral efficiency of optical communication systems [1–11]. A beam carrying OAM has a helical phase front, and its OAM order ℓ is defined as the number of 2π phase shifts in the azimuthal direction. Since OAM beams of different orders are theoretically orthogonal to one another, they could potentially be used as a modal basis set for efficient mode division multiplexing. The multiplexing and transmission of multiple data-carrying OAM beams has been experimentally demonstrated in free space, fibers, and underwater [1,2,5–11].

Approaches of transforming conventional Gaussian beams into OAM beams have included the use of following: (i) spiral phase plates (SPPs) [3,12,13]; (ii) computer-generated phase holograms with designed helical phase profiles [14,15]; (iii) inhomogeneous birefringent elements [16,17]; and (iv) metasurfaces [18–25]. Specifically, one such metasurface-based approach utilizes a thin dielectric metasurface phase mask, which has low loss, and is polarization insensitive in tailoring the wavefront of an incident beam [25]. However, questions remain unanswered concerning the operational implementation of such phase masks for generating data-carrying OAM beams.

In this Letter, we utilize such phase masks for the generation of OAM beams and demonstrate their performance over a OAM-multiplexing link. Performance of those phase masks is characterized by inspecting the impact of a nonzero beam's angle of incidence and lateral shift on the quality of the generated OAM modes. For certain scenarios, our results indicate that crosstalk introduced from the neighboring modes is less than −15 dB when tilt angle is limited to 20 deg, whereas lateral shift of 0.3 mm could cause a large amount of power leakage to adjacent modes of the desired channel. Additionally, a communication link multiplexing two OAM beams generated by the phase masks, each carrying a 40 Gbit/s data stream, is demonstrated [26].

The phase masks are fabricated using a dielectric metasurface platform based on amorphous Si (a-Si) nanoposts arranged in a hexagonal lattice on a fused silica glass substrate. The device used in this work has a lattice constant of 875 nm. The posts are of 1.2 μm in height and are cladded with cured SU-8 polymer, as shown in Fig. 1(a). Simulated transmission amplitude and phase for the array (at wavelength $\lambda = 1550$ nm) are shown in Fig. 1(b). The transmission phase can be changed from 0 to 2π by varying the post diameters in the range of 130–520 nm. Transmittance exceeds 97%, excluding the

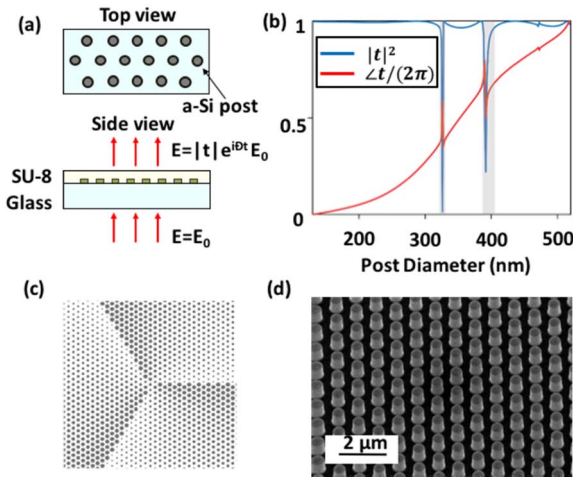

Fig. 1. (a) Schematic illustration of a periodic array of a-Si posts on a glass substrate. (b) Simulated transmission amplitude and phase of the array shown in (a) as a function of post diameter. (c) Pattern of posts with spatially varying diameters realizing an OAM generator with the topological charge of $\ell = +3$. (d) Scanning electron micrograph of a portion of a phase mask prior to SU-8 cladding.

resonances indicated by shaded rectangles in Fig. 1(b). For the generation of an OAM mode with a topological charge of ℓ, a phase mask with a spatially varying complex transmittance of $t(r, \varphi) = \exp(i\ell\varphi)$ is realized by sampling $t(r, \varphi)$ at the lattice sites and placing posts with diameters corresponding to the sampled phase at each site. The top view of such a phase mask for $\ell = +3$ is shown in Fig. 1(c). Spin-coated with a positive photoresist, the 1.2-μm-thick layer of a-Si is patterned using e-beam lithography. Then, a 70-nm-thick alumina layer is deposited on the photoresist by e-beam evaporation, followed by a liftoff process. The patterned alumina layer is subsequently used as a hard mask for dry etching of the a-Si layer. Next, the alumina mask is removed in a mixture of ammonia and hydrogen peroxide, and devices are cladded with SU-8 polymer. A scanning electron micrograph of a portion of a phase mask prior to SU-8 cladding is shown in Fig. 1(d).

Figures 2(a1) and 2(a2) show the intensity profiles of OAM beams generated by passing collimated Gaussian beams through the phase masks designed for OAM modes of $\ell = +1$ and $\ell = +3$, while Figs. 2(a3) and 2(a4) show their

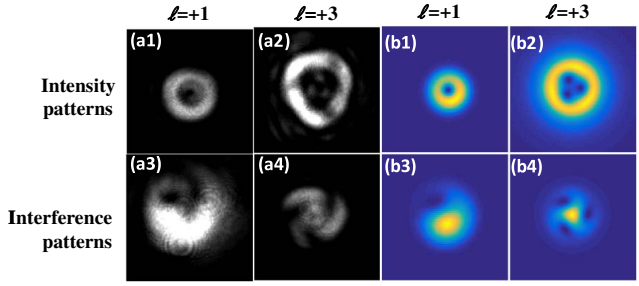

Fig. 2. OAM modes generated by passing Gaussian beams through phase masks. (a) Experiment results: intensity (a1 and a2) and interference patterns (a3 and a4) of OAM beams of $\ell = +1$ (left column) and $\ell = +3$ (right column) with a Gaussian beam. (b) Corresponding simulation results: intensity (b1 and b2) and interference patterns (b3 and b4).

corresponding interference patterns with a Gaussian beam. In these measurements, the diameter of the Gaussian beam is ~2.1 mm illuminating phase masks having a round shape with a diameter of 3 mm. Figure 2 shows the intensity and interference profiles of both experiment and simulation. We note the intensity profiles of the generated OAM beams, especially for $\ell = +3$, are somewhat triangular, probably caused by the interference of the main spatially modulated beam with a parasitically transmitted unmodulated portion of the incident Gaussian beam. This conjecture is supported by the simulation results of Fig. 3 for $\ell = +3$. As shown in the left-most inset, when the power ratio η of the unmodulated Gaussian beam is zero ($\eta = 0\%$), the simulated intensity pattern of OAM resumes a round ring shape with an intensity null at the center. When the power ratio of the unmodulated Gaussian beam increases (e.g., $\eta = 3\%$ or 10%), the intensity pattern is deformed from a ring to a triangle shape. This deformation can be potentially solved by reducing or deflecting the unmodulated Gaussian light. Since transmittance is already 97%, illustrated in Fig. 1(b), deflecting the unmodulated light could be a more effective solution. We also note that the experimental results do not exactly match the simulation results, possibly because of the following factors: (1) the distance of the simulation and experiment may be slightly different; and (2) the defections of the mirrors are not considered in the simulation.

To measure the quality of the generated OAM modes, we detect the power contents of modes other than the desired one at the receiver side and calculate that as the power leakage from the main mode. As depicted in Fig. 4(a), a phase-mask-generated OAM mode $\ell = +1$ experiences crosstalk of −17 dB from the $\ell = +3$ mode. Stronger crosstalk of −13 dB is observed [Fig. 4(c)] for the generated $\ell = +3$ OAM mode from mode $\ell = +1$. We also note higher mode purity (crosstalk less than −20 dB) is achieved for the same OAM modes when generated using a large, commercially available spatial light modulator (SLM), as shown in Figs. 4(b) and 4(d). We believe that increasing the fill factor (reducing spaces among pixels) of our phase mask may improve the purity of the generated OAM beams. Also, by adding a grating onto the spiral phase, the unmodulated Gaussian light may be deflected away, and the quality of the generated OAM beams may also be improved.

The phase masks are insensitive to the state of polarization of the incident Gaussian beam, as shown in Fig. 5. Here, the polarization direction of a constant power, linearly polarized incident beam is rotated while monitoring the power received at the intentionally generated OAM modes. For either $\ell = +1$

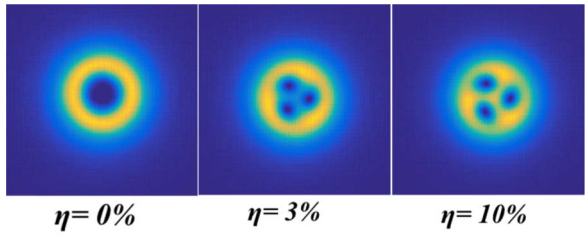

Fig. 3. Simulated intensity patterns of a phase-mask-generated OAM beam ($\ell = +3$) under three different power ratios of unmodulated incident Gaussian beam.

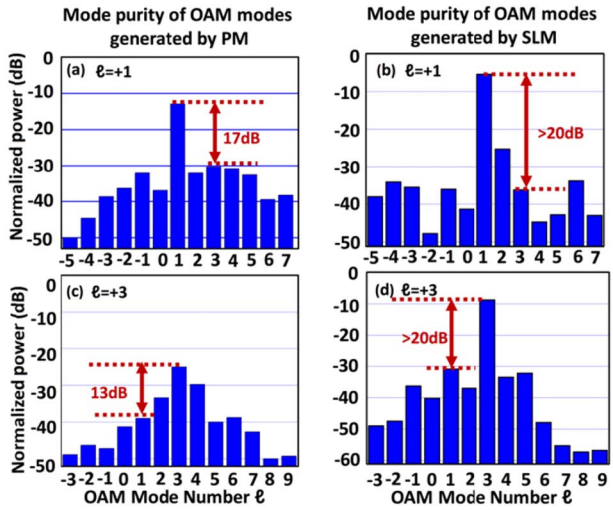

Fig. 4. Mode purity of OAM modes generated by both a phase mask and an SLM: (a) $\ell = +1$ by PM; (b) $\ell = +1$ by SLM; (c) $\ell = +3$ by PM; and (d) $\ell = +3$ by SLM. PM, phase mask; SLM, spatial light modulator.

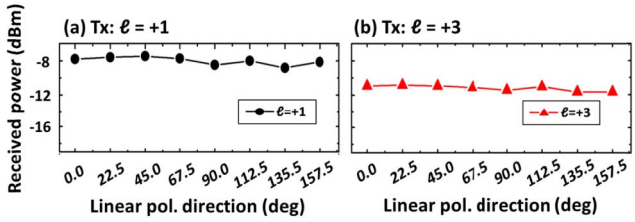

Fig. 5. Tolerance to the polarization states of the incident Gaussian beam: (a) when transmitting OAM beam $\ell = +1$; and (b) when transmitting OAM beam $\ell = +3$.

or $\ell = +3$ OAM mode, the polarization-dependent sensitivity (received power fluctuation) is less than 0.5 dB.

The effect of lateral misalignment between the normally incident Gaussian beam and phase mask is investigated with the setup of Fig. 6, where the SLM on the receiver side determines the quality of the generated OAM beams. The experiment is repeated when using SLM for OAM generation as a performance reference, as depicted by Figs. 7(b) and 7(d). The power of the desired OAM beam decreases and power leakage to neighboring modes increases significantly as the lateral misalignment increases. As shown by Fig. 7(a), when the

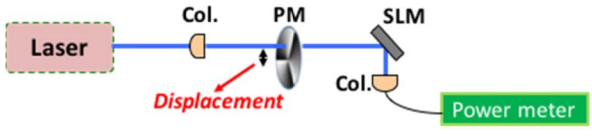

Fig. 6. Scheme to measure the tolerance to lateral displacement between the normally incident Gaussian beam and phase mask. The phase mask is used to generate the OAM beam while the SLM at the receiver side serves to filter specific modes for power measurement. SLM, spatial light modulator; Col., collimator; PM, phase mask.

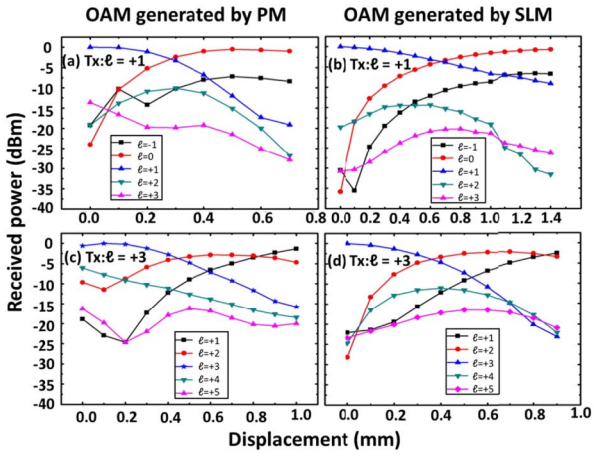

Fig. 7. Tolerance to lateral displacement between the normally incident Gaussian beam and phase mask. (a) Tx: $\ell = +1$, OAM generated by a phase mask. (b) Tx: $\ell = +1$, OAM generated by SLM. (c) Tx: $\ell = +3$, OAM generated by a phase mask. (d) Tx: $\ell = +3$, OAM generated by SLM. PM, phase mask; SLM, spatial light modulator.

phase-mask lateral displacement is 0.3 mm displacement (the size of the phase mask and incident beam are 3 mm and ~2.1 mm, respectively), the received power of the adjacent mode ($\ell = 0$) exceeds that of the desired one ($\ell = +1$).

Power leakage to neighboring modes may also increase with the angle of incidence between the incident Gaussian beam and the normal of the phase mask as shown in Fig. 8. Leakage weaker than −15 dB is observed for incident angles smaller than 20 deg. It seems that because the reason is that the phase profile imprinted to the incoming beam by a tiled phase mask is still close to a spiral when the tilt angle is small.

To investigate the performance of the phase-mask generated OAM beams in a communication link, a free space OAM multiplexing communication link is set up with a data rate of 80 Gbit/s employing those passive phase masks for OAM generation, as shown in Fig. 9. A data stream carrying 20 Gbaud quadrature-phase-shift-keying (QPSK) signal is generated and split into two branches, which are then converted to OAM carrying beams of modes $\ell = +1$ and $\ell = +3$. These two OAM channels are then multiplexed by a beam splitter. The propagation distance is 0.5 m, and an SLM is used at the receiver side

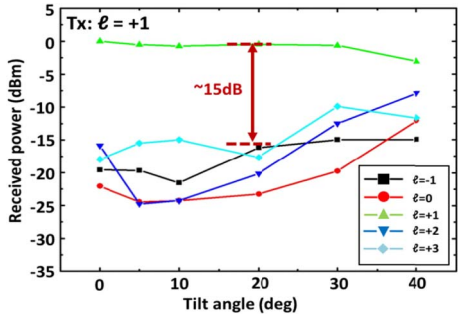

Fig. 8. Received power of transmitted and adjacent modes as a function of the tilt angle of the phase mask.

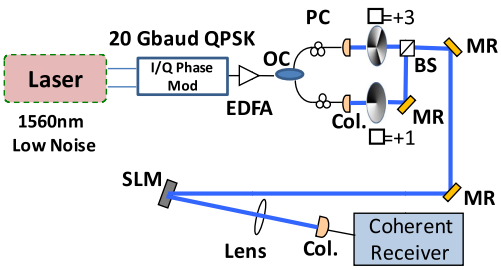

Fig. 9. Free space OAM multiplexing link with a data rate of 80 Gbit/s employing passive phase masks for OAM generation. EDFA, erbium-doped fiber amplifier; OC, optical coupler; MR, mirror; SLM, spatial light modulator; BS, beam splitter; Col., collimator; Mod., modulator.

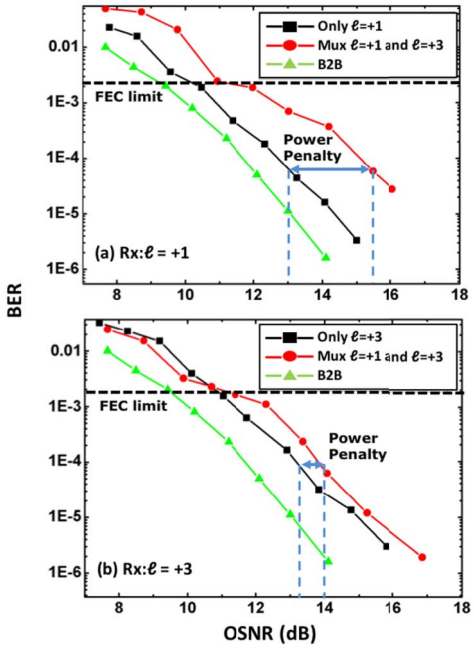

Fig. 10. BER measurement of 20 Gbaud QPSK signal on two OAM modes: (a) $\ell = +1$ and (b) $\ell = +3$.

to filter one channel at a time for BER detection. Figure 10 shows the BER of the two channels. The black line with solid square symbols shows the BER when only OAM $\ell = +1$ is transmitted. The power penalty shows up when we turn on channels $\ell = +1$ and $\ell = +3$ simultaneously, depicted by the red line with solid circles. The power penalty introduced from channel $\ell = +3$ to $\ell = +1$ [Fig. 10(a)] is higher than that from channel $\ell = +1$ to $\ell = +3$ [Fig. 10(b)].

Funding. Vannevar Bush Faculty Fellowship Program sponsored by the Basic Research Office of the Assistant Secretary of Defense for Research and Engineering and funded by the Office of Naval Research (ONR) (N00014-16-1-2813); National Science Foundation (NSF) (IIP-1622777); NxGen Partners; California Institute of Technology (Caltech) President's and Director's fund.

REFERENCES

1. G. Gibson, J. Courtial, M. J. Padgett, M. Vasnetsov, V. Pas'ko, S. M. Barnett, and S. Franke-Arnold, Opt. Express **12**, 5448 (2004).
2. H. Huang, G. Xie, Y. Yan, N. Ahmed, Y. Ren, Y. Yue, D. Rogawski, M. J. Willner, B. I. Erkmen, K. M. Birnbaum, S. J. Dolinar, M. P. J. Lavery, M. J. Padgett, M. Tur, and A. E. Willner, Opt. Lett. **39**, 197 (2014).
3. A. M. Yao and M. J. Padgett, Adv. Opt. Photon. **3**, 161 (2011).
4. S. Franke-Arnold, L. Allen, and M. Padgett, Laser Photon. Rev. **2**, 299 (2008).
5. J. Wang, J. Yang, I. M. Fazal, N. Ahmed, Y. Yan, H. Huang, Y. Ren, Y. Yue, S. Dolinar, M. Tur, and A. E. Willner, Nat. Photonics **6**, 488 (2012).
6. Y. Zhao, J. Liu, J. Du, S. Li, Y. Luo, A. Wang, L. Zhu, and J. Wang, *Optical Fiber Communications Conference* (2016), paper Th1H.3.
7. N. Bozinovic, Y. Yue, Y. Ren, M. Tur, P. Kristensen, H. Huang, A. E. Willner, and S. Ramachandran, Science **340**, 1545 (2013).
8. R. M. Nejad, K. Allahverdyan, P. Vaity, S. Amiralizadeh, C. Brunet, Y. Messaddeq, S. LaRochelle, and L. A. Rusch, J. Lightwave Technol. **34**, 4252 (2016).
9. K. Ingerslev, P. Gregg, M. Galili, F. D. Ros, H. Hu, F. Bao, M. A. U. Castaneda, P. Kristensen, A. Rubano, L. Marrucci, S. Ramachandran, K. Rottwitt, T. Morioka, and L. K. Oxenløwe, *Optical Fiber Communications Conference* (2017), paper M2D.1.
10. J. Baghdady, K. Miller, K. Morgan, M. Byrd, S. Osler, R. Ragusa, W. Li, B. M. Cochenour, and E. G. Johnson, Opt. Express **24**, 9794 (2016).
11. Y. Ren, L. Li, Z. Wang, S. M. Kamali, E. Arbabi, A. Arbabi, Z. Zhao, G. Xie, Y. Cao, N. Ahmed, Y. Yan, C. Liu, A. J. Willner, S. Ashrafi, M. Tur, A. Faraon, and A. E. Willner, Sci. Rep. **6**, 33306 (2016).
12. M. W. Beijersbergen, R. P. C. Coerwinkel, M. Kristensen, and J. P. Woerdman, Opt. Commun. **112**, 321 (1994).
13. S. Oemrawsingh, J. Van Houwelingen, E. R. Eliel, J. P. Woerdman, E. J. K. Verstegen, and J. G. Kloosterboer, Appl. Opt. **43**, 688 (2004).
14. N. R. Heckenberg, R. McDuff, C. P. Smith, and A. G. White, Opt. Lett. **17**, 221 (1992).
15. A. Forbes, A. Dudley, and M. McLaren, Adv. Opt. Photon. **8**, 200 (2016).
16. L. Marrucci, C. Manzo, and D. Paparo, Phys. Rev. Lett. **96**, 163905 (2006).
17. G. Milione, M. Lavery, H. Huang, Y. Ren, G. Xie, T. Nguyen, E. Karimi, L. Marrucci, D. Nolan, R. Alfano, and A. Wilner, Opt. Lett. **40**, 1980 (2015).
18. Z. Zhao, J. Wang, S. Li, and A. E. Willner, Opt. Lett. **38**, 932 (2013).
19. Y. Yang, W. Wang, P. Moitra, I. I. Kravchenko, D. P. Briggs, and J. Valentine, Nano Lett. **14**, 1394 (2014).
20. M. Pu, X. Li, X. Ma, Y. Wang, Z. Zhao, C. Wang, C. Hu, P. Gao, C. Huang, H. Ren, and X. Li, Sci. Adv. **1**, e1500396 (2015).
21. N. Yu, P. Genevet, M. A. Kats, F. Aieta, J. Tetienne, F. Capasso, and Z. Gaburro, Science **334**, 333 (2011).
22. P. Genevet, N. Yu, F. Aieta, J. Lin, M. A. Kats, R. Blanchard, M. O. Scully, Z. Gaburro, and F. Capasso, Appl. Phys. Lett. **100**, 013101 (2012).
23. J. Lin, P. Genevet, M. A. Kats, N. Antoniou, and F. Capasso, Nano Lett. **13**, 4269 (2013).
24. S. Vo, D. Fattal, W. V. Sorin, Z. Peng, T. Tran, M. Fiorentino, and R. G. Beausoleil, IEEE Photon. Technol. Lett. **26**, 1375 (2014).
25. A. Arbabi, Y. Horie, M. Bagheri, and A. Faraon, Nat. Nanotechnol. **10**, 937 (2015).
26. Z. Wang, Y. Yan, A. Arbabi, C. Liu, G. Xie, Z. Zhao, Y. Ren, L. Li, N. Ahmed, A. Willner, E. Arbabi, A. Faraon, N. Ashrafi, S. Ashrafi, M. Tur, and A. E. Willner, *Conference on Lasers and Electro-Optics* (2016), paper SW4F.5.